Applied Catalysis B: Environmental 250 (2019) 31–41

Contents lists available at ScienceDirect

Applied Catalysis B: Environmental

journal homepage: www.elsevier.com/locate/apcatb

Highly efficient Z-scheme structured visible-light photocatalyst constructed by selective doping of Ag@AgBr and Co_3O_4 separately on {010} and {110} facets of $BiVO_4$: Pre-separation channel and hole-sink effects

Fangfei Chen[a], Chaoyue Wu[a], Jinnan Wang[a,*], Corvini Philippe François-Xavier[b], Thomas Wintgens[b]

[a] State Key Laboratory of Pollution Control and Resource Reuse, School of the Environment Nanjing University, Nanjing, 210023, China
[b] School of Life Sciences, University of Applied Sciences and Arts Northwestern Switzerland, Basel, 4132, Switzerland

ARTICLE INFO

Keywords:
Z-Scheme
Ag@AgBr/$BiVO_4$/Co_3O_4
Visible-light photocatalyst
Pre-separation channel
Hole-sink effect

ABSTRACT

To improve the visible-light photocatalytic activity and photo-carriers separation of $BiVO_4$, highly efficient Z-scheme structured visible-light photocatalyst Ag@AgBr/$BiVO_4$/Co_3O_4 was constructed by selective doping of Ag@AgBr and Co_3O_4 on {010} and {110} facets of $BiVO_4$. Due to the different energy levels of conduction band (CB) and valence band (VB) between {010} facet and {110} facet, $BiVO_4$ could act as the 'pre-separation channel' to achieve spatial charge separation. Such pre-separation channel effect improved photo-electrons transfer from $BiVO_4${010} facets to electron mediator (Ag°) for subsequent recombination with holes of AgBr. Thus, the photo-induced electrons of AgBr could be accumulated on CB for reduction of O_2 to $^{\cdot}O_2^-$. On the other hand, holes of $BiVO_4$ accumulated on {110} facets were captured by deriving-hole-type co-catalysts Co_3O_4 for organics oxidation. In addition, Ag° not only served as the electron mediator of Z-scheme but also improve the visible-light utilization due to SPR-effect. Being attributed to the synergistic effect of pre-separation channel and deriving-hole-type co-catalysts, Z-scheme structured Ag@AgBr/$BiVO_4$/Co_3O_4(0.15 wt%) achieved high photo-degradation rate of organics. Even after 9th cycles, Ag@AgBr/$BiVO_4$/Co_3O_4(0.15 wt%) could still photo-degraded more than 90% of OTC within 24 min. DRS, PL and photoelectrochemical analyses also confirmed the improvement of visible-light utilization and charge separation of Ag@AgBr/$BiVO_4$/Co_3O_4. The radical trapping experiments and EPR demonstrated that both superoxide radical ($^{\cdot}O_2^-$) and holes (h^+) were main active species for organics photodegradation. In summary, this work not only constructed a highly efficient Z-scheme structured visible-light photocatalyst, but also provided a new method to diminish the photo-carriers recombination by pre-separation channel and hole-sink effects.

1. Introduction

As visible-light photocatalysts, Bi-based photocatalysts [1–5] and Ag-based photocatalysts [6–11] attract people's attention in recent years. Among them, monoclinic scheelite bismuth vanadate (m-$BiVO_4$) was considered as the one of the most promising photocatalyst for water oxidation and organics degradations due to high theoretical solar-to-hydrogen conversion efficiency (9.2%) and photocurrent (7.5 mA cm^{-2} under standard AM 1.5 solar light irradiation) [12], chemical stability [13] and nontoxicity [14]. However, the practical photocatalytic efficiency of $BiVO_4$ is much lower than what is expected because of relatively low visible-light utilization [15] and inefficient charge separation [16]. About 60%–80% of the photo-carriers recombined before they reached the interfaces, which significantly decreased the photocatalytic activity of $BiVO_4$ [12]. Thus, it is expected to improve the catalytic activity of $BiVO_4$ by enhancement of visible-light utilization and charge separation.

To enhance visible-light utilization, redox ability and photo-carrier separation, photocatalysts should possess lower band gaps, more positive VB and negative CB potentials and diminished charge recombination rate [17]. However, as for single-component semiconductor, more positive VB and negative CB potentials suggested a wider band gap, which could not exhibit high visible-light utilization. To resolve this problem, Z-scheme structured photocatalysts were constructed by combination of Photosystem I (PS I) and Photosystem II (PS II). Photo-electrons in the CB of PS II were transferred to the electron mediator

* Corresponding author.
E-mail address: wjnnju@163.com (J. Wang).

https://doi.org/10.1016/j.apcatb.2019.03.023
Received 3 January 2019; Received in revised form 4 March 2019; Accepted 9 March 2019
Available online 09 March 2019
0926-3373/

(noble heavy metal particles or RGO), and subsequently recombined with holes in the VB of PS I. Such charge transfer not only improved the photo-carriers separation, but also achieved strong reducibility of PS I and oxidizability of PS II [18]. Meanwhile, due to a narrower band gap, Z-scheme photocatalytic system had a wider visible-light-responsive range, which enhanced the visible-light utilization [19].

Among Ag-based photocatalyst, Ag/AgX (Cl, Br and I) exhibited excellent photocatalytic performance due to their favorable charge carrier mobility [20–23]. More importantly, as noble metal particle, Ag° could not only possess surface plasmon resonance (SPR) effect [24,25] but also act as the electron mediator in Z-scheme system, with successful cases such as Ag_3PO_4/Ag/$BiVO_4$ [13], g-C_3N_4/Ag/$BiVO_4$ [26], AgBr/Ag/$PbBiO_2Br$ [27]. Wu.et.al constructed the Z-scheme structured Ag@AgCl/$BiVO_4$ which possessed high photocatalytic activity and stability [28]. Jiang.et.al prepared the Z-scheme structured photocatalyst Ag/AgCl@MIL-53-Fe for simultaneous organics oxidization and Cr (VI) reduction [29]. Compared with AgCl (E_g = 3.25 eV) [28], AgBr had a more narrow band gap (2.6 eV) so that it can be excited by visible-light [30]. Niu et al. fabricated the novel Z-scheme structured CeO_2–Ag/AgBr which showed excellent visible light photocatalytic activity for CIP photodegradation [31]. Liu et al. synthesized the Z-scheme $ZnFe_2O_4$/AgBr/Ag composites, in which $ZnFe_2O_4$ and AgBr could be excited under visible-light irradiation [32]. Yang.et.al constructed the Z-scheme photocatalyst Ag/AgBr/$BiVO_4$ which could simultaneously reduce Cr(VI) and oxidize organics [24]. However, the random charge migration from the bulk to surface of each semiconductor inevitably induced serious self-recombination, which might decrease the photocatalysts activity and stability [33]. Thus, adding a 'pre-separation process' of photo-electrons and holes before their migration from the bulk to surface of each semiconductor in Z-scheme system can prevent their self-recombination. Fortunately, $BiVO_4$ could act as pre-separation channel due to the different energy levels of the CB and VB between {010} and {110} facets. Thus, photo-electrons and holes were spatially separated and accumulated on {010}facet and {110}facet, respectively [34]. With this pre-separation channel effect of $BiVO_4$, it is expected to construct the Z-scheme system (Ag@AgBr/$BiVO_4$) by doping Ag@AgBr onto $BiVO_4$ {010} facet. In Ag@AgBr/$BiVO_4$, photo-electrons (accumulated on {010} facet) of $BiVO_4$ can be transferred to Ag° and subsequently recombined with photo-generated holes in the VB of AgBr. As a result, the photo-electrons can be accumulated in the CB of AgBr for reduction O_2 to $^{\cdot}O_2^-$.

On the other hand, co-catalyst doped on photocatalyst could not only enhance quantum efficiency by trapping photo-generated charges for promotion of the charge separation [5], but also lower the activation energy of reaction [35]. Co-catalysts are usually classified into two groups: deriving-hole-type co-catalysts and deriving-electron-type co-catalysts [36]. Since the VB top level of $BiVO_4$ (2.7 eV vs SHE) is relatively high, photo-induced holes are the main active species for organics degradation. Thus, selectively loading deriving-hole-type co-catalysts onto hole-rich {110} facet of $BiVO_4$ could facilitate the accumulation of holes for organics oxidation. Compared with other deriving-hole-type co-catalysts (MnO_x [36], PbO_2 [34] and RuO_2 [37]), Co_3O_4 possess stronger hole-sink effect [38]. Fan et al. doped Co_3O_4 on Ag_3PO_4 for improvement of the visible light photocatalytic activity [38]. Li et al. demonstrated that photocatalytic water oxidation was significantly enhanced by doping Pt and Co_3O_4 onto different facets of $BiVO_4$ [39]. Thus, it is expected to modulate the photo-generated holes of $BiVO_4$ for improvement of charge separation by selectively depositing deriving-hole-type co-catalysts Co_3O_4 on {010} facets of $BiVO_4$.

Based on the research background mentioned above, we constructed novel Z-scheme structured Ag@AgBr/$BiVO_4$/Co_3O_4 composites by selective deposition of Ag@AgBr and Co_3O_4 on {010} and {110} facets of $BiVO_4$. In Ag@AgBr/$BiVO_4$/Co_3O_4 composite, due to the different energy levels of CB and VB between {010} and {110} facets, $BiVO_4$ can act as the 'pre-separation channel' to achieve spatial charge separation. Notably, photo-electrons (accumulated on {010} facet) of $BiVO_4$ can be transferred to Ag° and subsequently recombined with photo-generated holes in the VB of AgBr, which facilitate the photo-electrons accumulated in CB of AgBr for reduction O_2 to $^{\cdot}O_2^-$. Furthermore, as noble metal particle, Ag° could not only serve as the electron mediator of Z-scheme, but also enhance the visible-light utilization due to SPR-effect. In addition, since holes were accumulated on {110} facets of $BiVO_4$, the selective decoration of deriving-hole-type co-catalysts Co_3O_4 on hole-rich facets {110} could capture holes for organics oxidation. Thus, visible-light photocatalytic activity and charge separation were significantly improved. In order to evaluate the potential of Ag@AgBr/$BiVO_4$/Co_3O_4, our current work focused on four aspects as follows: 1) to construct Z-scheme structured visible-light photocatalyst by selective deposition of Ag@AgBr and Co_3O_4 on {010} and {110} facet of $BiVO_4$; 2) to characterize this novel visible-light photocatalyst by using FE-SEM, XPS, XRD, DRS, PL and photoelectrochemical analyses; 3) to evaluate the visible-light photocatalytic activity and stability; and 4) to propose the possible photocatalytic mechanisms.

2. Experimental

2.1. Chemicals

Chemicals [Bi $(NO_3)_3{\cdot}5H_2O$, NH_4VO_3, Co $(NO_3)_2{\cdot}6H_2O$, $NaIO_3$, $(NH_4)_2C_2O_4$, $AgNO_3$] used in this experiment were analytical grade (Aladdin Corporation, shanghai, China).

2.2. Synthesis of Ag@AgBr/$BiVO_4$/Co_3O_4

2.2.1. Synthesis of decahedron $BiVO_4$

Decahedron $BiVO_4$ with {110} and {010} facets was synthesized following the method reported in previous literature [34]. Typically, 6 mmol Bi $(NO_3)_3{\cdot}5H_2O$ and NH_4VO_3 were dissolved in 200 mL HNO_3 solution (2 M). Then, $NH_3{\cdot}H_2O$ (25%) was added into the solution for adjustment of pH to 2.0 under stirring with production of orange precipitate. After aging for 2 h, the orange precipitate was transferred to a 100 mL Teflon-lined stainless steel autoclave and subsequently heated at 200 ℃ for 12 h. The vivid yellow powder (decahedron $BiVO_4$) was obtained, and then separated by filtration, washed with DI water for several times. Before use, the decahedron $BiVO_4$ was dried at 60 ℃ in vacuum oven.

2.2.2. Selective photo-deposition of Co_3O_4 on {110} facet of $BiVO_4$

Due to the different energy levels of CB and VB between {010} facet and {110} facet, holes were accumulated on the {110} facet of $BiVO_4$. Thus, selective photo-deposition of Co_3O_4 on {110} facet of $BiVO_4$ was achieved with Co $(NO_3)_2{\cdot}6H_2O$ as the precursor, and $NaIO_3$ was employed as the photo-electron acceptors. Typically, 0.50 g decahedron $BiVO_4$ was added in 100 ml $NaIO_3$ solutions (0.01 M) with ultrasonic treatment for 15 min. Certain amount of Co $(NO_3)_2$ solution (0.50 g·L^{-1}) was added in the suspension which was then irradiated by a 300 W Xe lamp ($\lambda > 420$ nm) under the stirring. After 3 h photo-deposition reaction, the suspension was filtered, washed with DI water for more than 3 times, and finally dried at 60 ℃. In this way, samples with different weight ratios of Co_3O_4 to $BiVO_4$ (i.e., 0.02 wt%, 0.05 wt%, 0.1 wt%, 0.15 wt%, 0.2 wt%, 0.5 wt% Co_3O_4/$BiVO_4$) were prepared.

2.2.3. Selective deposition of Ag@AgBr on {010} facet of $BiVO_4$

In order to comparative study the effect of Co_3O_4 on photocatalytic performance, Ag@AgBr/$BiVO_4$ was synthesized as following method.

(1) Preparation of Ag/$BiVO_4$: Due to the different energy levels of CB and VB between {010} facet and {110} facet, photo-electrons were accumulated on the {010} facet of $BiVO_4$. Thus, selective photo-deposition of Ag° on {010} facet of $BiVO_4$ was achieved with $AgNO_3$ as the precursor, and $(NH_4)_2C_2O_4$ was employed as holes acceptors. Typically, 0.50 g $BiVO_4$ was added to $(NH_4)_2C_2O_4$ solution (0.8 g L^{-1}, 100 mL) in a 250 mL beaker with ultrasonic treatment. Then, certain amount of

$AgNO_3$ was added into the solution under stirring. By irradiation of 300 W Xe lamp (λ > 420 nm) for 2 h, the color of mixture turned from vivid yellow to grayish-green, which indicated the photo-reduction of Ag^+ to Ag°. After centrifugation and filtration, the filter residue (Ag/$BiVO_4$) was washed with DI water and then dried at 60 ℃.

(2) Preparation of Ag@AgBr /$BiVO_4$: 0.50 *g* Ag/$BiVO_4$ composite was added in certain amounts of Fe $(NO_3)_3$ solution (0.1 mol L^{-1}), then the same amount of 0.1 mol L^{-1} NaBr solution was added to the mixture under stirring for 4 h. With the oxidation of Ag° to AgBr nanoparticles, the color of precipitant gradually turned from dark green to greenish yellow. After centrifugation and filtration, the filter residue (Ag@AgBr/$BiVO_4$) was washed with DI water and then dried at 60 ℃.

2.2.4. Construct Z-scheme structured Ag@AgBr/$BiVO_4$/Co_3O_4

The Z-scheme structured Ag@AgBr/$BiVO_4$/Co_3O_4 composites was constructed by sequential decomposition of Co_3O_4 and Ag@AgBr separately on {110} and {010} facets of $BiVO_4$. Firstly, Co_3O_4/$BiVO_4$ was synthesized by selective photo-deposition of Co_3O_4 on $BiVO_4${110} facet, which followed the methods of Section 2.2.2. Then Ag@AgBr/$BiVO_4$/Co_3O_4 was fabricated by selective decoration of Ag@AgBr on $BiVO_4${010} facet by the method of Section 2.2.3.

2.3. Characterization of Ag@AgBr/$BiVO_4$/Co_3O_4

The morphology and microstructure of the samples were characterized using scanning electron microscope (SEM, QUANTA FEG 250). To determine the composition of samples, energy dispersive spectroscopy (EDS) mapping images were also captured. The crystal phases of samples were recorded on the X-ray diffractometer (Cu-kα radiation, X'TRA, Switzerland) in the range of 10–80° (2θ) at a scanning rate of 5° min^{-1}. Furthermore, surface chemical composition and states of photocatalysts were analyzed by X-ray photoelectron spectroscopy (XPS, PHI 5000 VersaProbe III with AES, ULVAC-PHI, Japan) with an Al-kα X-ray source. The photoelectrochemical analyses were performed on the electrochemical workstation (CHI760E, China) with a conventional three-electrode system. To evaluate the separation efficiency of electron-hole pairs in photocatalysts, the photoluminescence (PL) spectra were detected using Fluorescence spectrometry (Horiba HJY FM4P-TCSPC). In addition, the UV–vis diffuse reflectance spectra (DRS) were analyzed by integrating sphere attached to UV–vis spectrophotometer (UV-3600, Shimadzu, Japan), which could provide useful information of catalysts optical properties.

2.4. Photocatalytic activity tests

Photocatalytic degradation of rhodamine B (RhB) was carried out for evaluation of catalytic activity in the XPA-VII photocatalytic reactor (Xujiang Electromechanical Plant, Nanjing, China). A 350 W Xe lamp irradiation with a 420 nm cut-off filter to remove light of λ < 420 nm (light intensity: 108.2 mW/cm^2) placed axially at the center of the quartz immersion was employed as the visible-light source. To confirm the optimization contents of AgBr and Co_3O_4 in Ag@AgBr/$BiVO_4$/Co_3O_4 composite, photocatalytic activity of various photocatalysts with different AgBr contents (2 wt%–20 wt%) and different Co_3O_4 contents (0.02 wt%–0.5 wt%) were tested as follows: 0.05 g photocatalyst was added into 50 ml RhB aqueous solution (10 mg L^{-1}). Before illumination, the suspensions were magnetically stirred in dark for 30 min to reach absorption-desorption equilibrium between the photocatalysts and RhB (Fig. S1). During the photo-degradation process, 3 ml suspensions were withdrawn periodically, followed by centrifugation (3500 rpm) to separate the photocatalyst. Then, the residual concentration of RhB in solution was measured by using the UV–vis spectrophotometer (wavelength = 554 nm). As a comparison, the photocatalytic degradation experiments over different photocatalysts ($BiVO_4$, Co_3O_4/$BiVO_4$, Ag@AgBr/$BiVO_4$) were also conducted using the same method. The photocatalytic degradation rate (*E%*) was calculated according to the equation of $[E\% = (C_0 - C)/C_0 \times 100\%]$, where C_0 (mg L^{-1}) is the initial concentration of RhB and C (mg L^{-1}) is the residual concentration of RhB after photo-degradation.

In addition, to evaluate the photocatalytic stability of Ag@AgBr/$BiVO_4$/Co_3O_4, 9 successive cycles of photo-degradation of oxytetracycline (OTC) were conducted as photo-degradation experiment of RhB, except for that photocatalyst were reused after each cycle. 1.5 ml suspensions were withdrawn periodically, and the catalysts were filtrated by 0.22 μm cellulose acetate membrane before determination. The residual concentration of OTC in solution was measured by using high performance liquid chromatography (HPLC, Agilent, America). The photo-degradation intermediates of OTC were analyzed by HPLC coupled with time-of-flight mass spectrometry detection (HPLC–TOFMS, Agilent 1290 Infinity LC/6460 QQQ MS, America) in positive polarity. Supplementary material (Table S1) listed the operating conditions of HPLC and HPLC-TOFMS in details.

2.5. Photocatalytic mechanism of Ag@AgBr/$BiVO_4$/Co_3O_4

To deeply elucidate the photocatalytic mechanism, trapping free radicals experiments were conducted to identify the main active species. Ethylenediamine tetra acetic acid disodium salt (EDTA-2Na), *tert*-butanol (BuOH) and p-benzoquinone (BQ) can be used to trap the active species generated in the photocatalytic system, by which we could preliminarily demonstrate the main reactive oxidative species. Following the method in Section 2.4, EDTA-2Na (10 mM), tBuOH (10 mM) and *p*-benzoquinone (10 mM) were respectively added into RhB (10 mg L^{-1}) solution before photo-degradation. In addition, 5, 5-dimeyhyl-1-pyrroline-*N*-oxide (DMPO) was used as the spin trap, and electron paramagnetic resonance (EPR) spectra of photocatalysts ($BiVO_4$, Co_3O_4/$BiVO_4$, Ag@AgBr/$BiVO_4$, Ag@AgBr/$BiVO_4$/Co_3O_4) were recorded on an EMX-10/12 (Bruker, Germany) with a Xe lamp.

3. Results and discussion

3.1. Structure and morphology of Ag@AgBr/$BiVO_4$/Co_3O_4

3.1.1. SEM analysis

The microstructures and morphologies of Ag@AgBr/$BiVO_4$/Co_3O_4 composite were characterized by FESEM. The sample of $BiVO_4$ exhibits a decahedron crystal structure with relatively smooth surface and sharp edges (Fig. 1a), which is similar to standard decahedron $BiVO_4$ reported in previous literature [28]. The sides of the regular decahedron $BiVO_4$ are {110} facets, while the bottom and top surfaces are {010} facets [34]. Due to the different energy levels of the CB and VB between {010} and {110} facets, the photogenerated electrons and holes tended to accumulate on {010} and {110} facets of $BiVO_4$, respectively. Thus, a thin layer of Co_3O_4 is deposited on {110} facets of $BiVO_4$ crystals by photo-oxidization reaction (Fig. 1b), confirming the successful preparation of Co_3O_4/$BiVO_4$. Subsequently, Ag@AgBr is selectively deposited on the top and bottom surfaces of Co_3O_4/$BiVO_4$ (Fig. 1c) by the following reactions (Fig. 1d): (1) photo-reduction of Ag^+ to Ag° particles on the top and bottom surfaces of Co_3O_4/$BiVO_4$; (2) owing to a higher redox potential of Fe^{3+}/Fe^{2+} (+0.771 V vs. SHE) than Ag^+/Ag° (+0.223 V vs. SHE) [40], $Fe(NO_3)_3$ oxidize Ag° particles to Ag^+ which subsequently in situ form core-shell structure of Ag@AgBr by reaction with NaBr. Thus, in the composite of Ag@AgBr/$BiVO_4$/Co_3O_4, Co_3O_4 and Ag@AgBr are selectively deposited on {110} and {010} facets of $BiVO_4$, which can be confirmed by the EDS images (Fig. 1e). As a comparison, the Ag@AgBr/$BiVO_4$ composite is also synthesized (Fig. 1f).

3.1.2. XRD analysis

The purity and crystal structures of $BiVO_4$, Co_3O_4/$BiVO_4$, Ag@AgBr/$BiVO_4$ and Ag@AgBr/$BiVO_4$/Co_3O_4 were analyzed by XRD spectra. It indicates that pure $BiVO_4$ powder is well matched with the

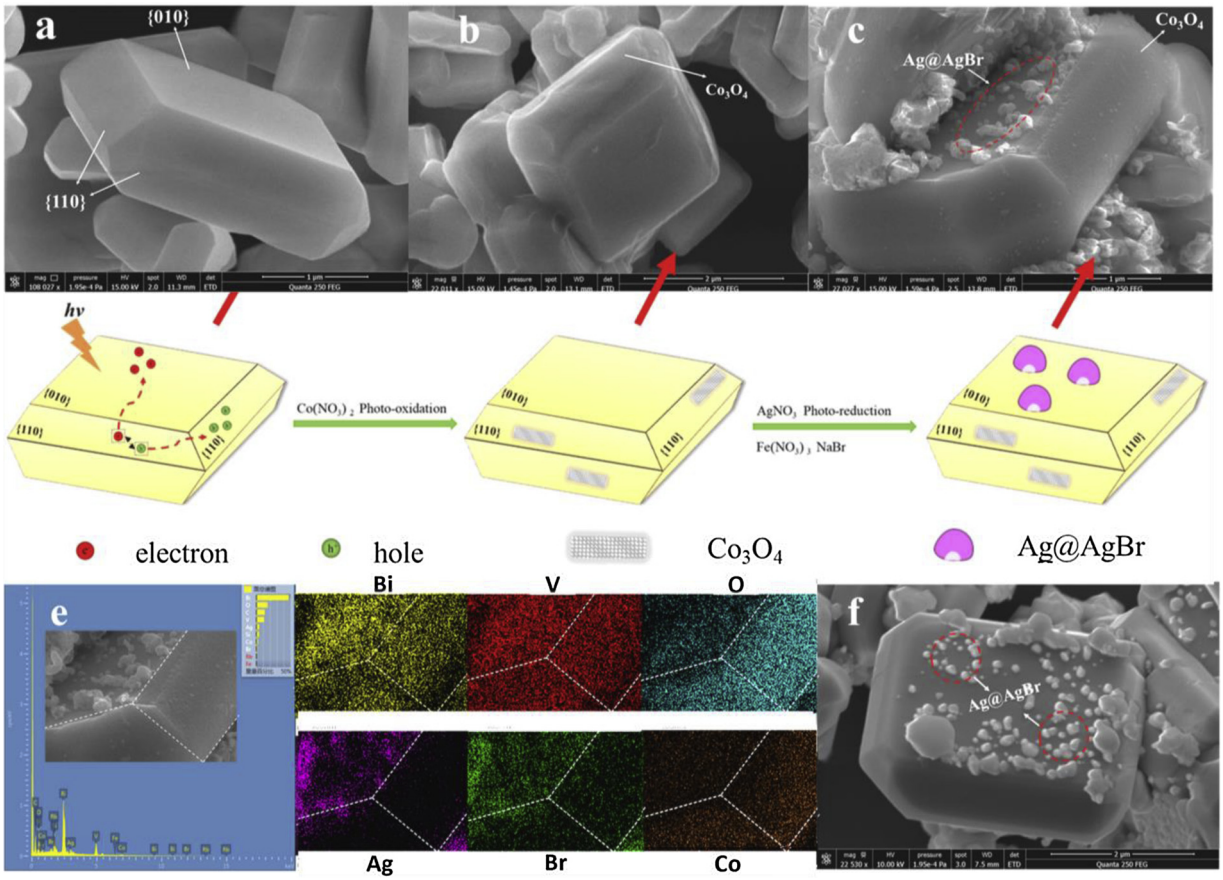

Fig. 1. SEM images of photocatalysts (a) $BiVO_4$, (b) $Co_3O_4/BiVO_4$ and (c) $Ag@AgBr/BiVO_4/Co_3O_4$. (d) Synthesis process of photocatalysts. (e) Element mapping images for Bi, V, O, Ag, Br, and Co in $Ag@AgBr/BiVO_4/Co_3O_4$ composites. (f) SEM image of $Ag@AgBr/BiVO_4$.

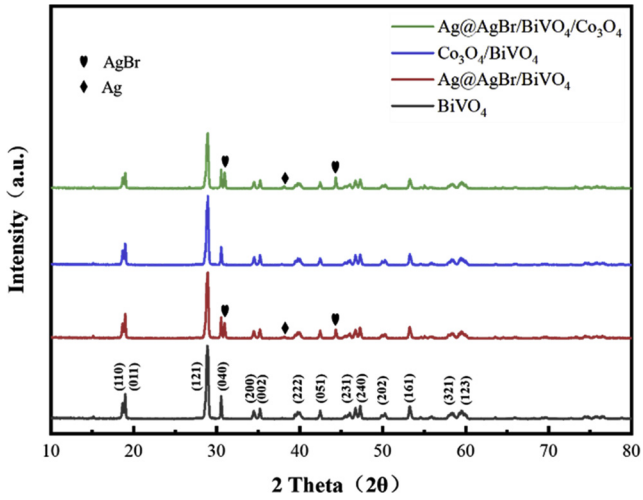

Fig. 2. XRD patterns of $BiVO_4$, $Co_3O_4/BiVO_4$, $Ag@AgBr/BiVO_4$ and $Ag@AgBr/BiVO_4/Co_3O_4$(0.15 wt%).

monoclinic phase of $BiVO_4$ (JCPDS NO. 14-0688) (Fig. 2) [13,28]. The diffraction peaks at 18.6°, 18.9°, 28.9°, 30.5°, 34.4°, 35.1°, 39.9°, 42.5°, 45.9°, 47.2°, 50.3°, 53.3°, 58.4°and 59.7° are ascribed to the (110), (011), (121), (040), (200), (002), (222), (051), (231), (240), (202), (161), (321) and (123) diffraction phases of $BiVO_4$, respectively. The diffraction peaks of AgBr near 30.9° and 44.3° are assigned to (200) and (220) crystal phases in accordance to the diffractions of crystalline AgBr (JCPDS No. 06-0438) [24]. The peak near 38.1° is ascribed to the (111) crystal phases of Ag (JCPDS No. 04-0783) [24,41]. Since the content of poor crystalline Co_3O_4 nanoparticles is low, the diffraction peaks of Co_3O_4 could be hardly observed on the XRD patterns. After decomposition of Ag@AgBr and Co_3O_4, the diffraction peak of $BiVO_4$ was not changed, which indicated that Ag@AgBr and Co_3O_4 did not destroy the crystal structure of $BiVO_4$.

3.1.3. X-ray photoelectron spectroscopy (XPS)

In order to identify the existence of Co_3O_4 and the chemical state of photocatalyst, XPS spectra was used to analyze the $BiVO_4$, $Co_3O_4/BiVO_4$, $Ag@AgBr/BiVO_4$ and $Ag@AgBr/BiVO_4/Co_3O_4$(0.15 wt%). Fig. 3a shows the survey scan spectra of as-prepared photocatalysts. As for $Ag@AgBr/BiVO_4/Co_3O_4$(0.15 wt%) composite, XPS scan signals originating from Br 3d, Bi 4f, Ag 3d, V 2p, O 1s, and Co 2p, are respectively identified at binding energies of 69 eV, 157 eV, 371 eV, 515.6 eV, 531.8 eV and 779.5 eV. In Fig. 3b, the binding energies around 779.5 eV is corresponding to Co 2p3 levels, which indicates that Co_3O_4 has been successfully doped on $BiVO_4$ and $Ag@AgBr/BiVO_4$. O 1 s peaks of $Co_3O_4/BiVO_4$ and $Ag@AgBr/BiVO_4/Co_3O_4$(0.15 wt%) can be deconvoluted into two peaks at 531 eV and 529 eV (Fig. 3c) which belong to the V−O bonds [28,42] and Co−O bond [43,44], respectively. This result also confirmed the successful decomposition of Co_3O_4 on $BiVO_4$, although XRD patterns did not show obvious diffraction peaks of Co_3O_4. As shown in Fig. 3d, two strong peaks at 367.2 eV and 373.4 eV are assigned to Ag^+ of AgBr [45], while peaks at 368.0 eV and 374.2 eV correspond to Ag° of $Ag@AgBr/BiVO_4$ and $Ag@AgBr/BiVO_4/Co_3O_4$(0.15 wt%) [24]. Thus, SEM, XRD and XPS results well demonstrated that Ag@AgBr and Co_3O_4 had been selectively deposited on {010} and {110} facets of $BiVO_4$, respectively.

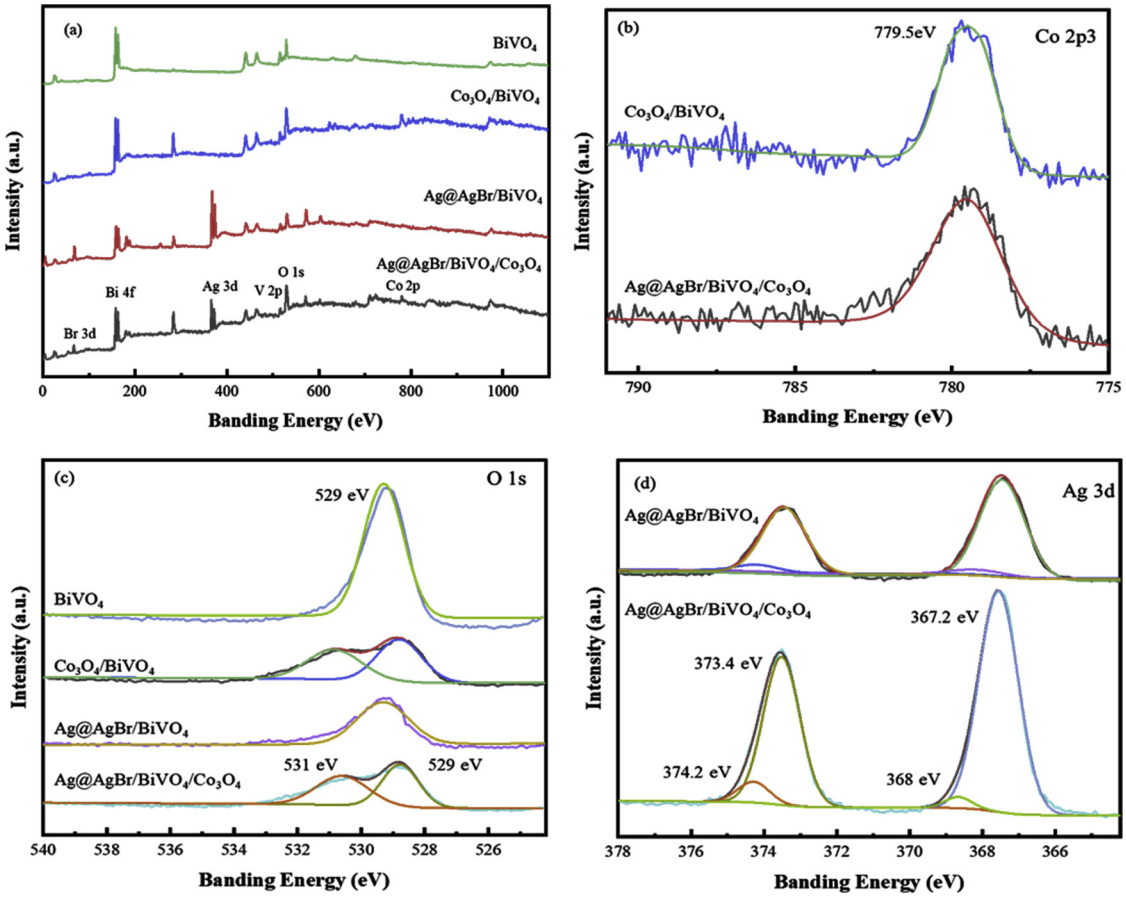

Fig. 3. XPS spectra of as-prepared samples. (a) Survey, (b) Co 2p3, (c) O 1 s, (d) Ag 3d.

3.2. Optical properties of the Z-scheme structured $Ag@AgBr/BiVO_4/Co_3O_4$

UV–vis diffuse reflectance spectra (DRS) of $BiVO_4$, $Co_3O_4/BiVO_4$, $Ag@AgBr/BiVO_4$ and $Ag@AgBr/BiVO_4/Co_3O_4$ are measured to characterize their optical properties (Fig. 4a). Being attributed to the intrinsic band gap absorption, pure $BiVO_4$ has strong absorption at short wavelength (< 500 nm). As a visible-light induced semiconductor, Co_3O_4 doped on {110} facets of $BiVO_4$ could enhance the visible-light absorption. Thus, $Co_3O_4/BiVO_4$ showed much higher visible-light response than pure $BiVO_4$. Notably, after Ag@AgBr doped on $Co_3O_4/BiVO_4$, absorbance in the visible region (> 500 nm) was significantly enhanced. Such improvement might be attributed to the surface plasmon resonance (SPR) effect of Ag° and the Z-scheme structure of $Ag@AgBr/BiVO_4/Co_3O_4$ composite. This inference was proved by band gap energy (E_g) which could be calculated according to the equation of $[\alpha h\upsilon = A\ (h\upsilon - E_g)^n]$. Where α is the absorption coefficient, h is Planck's constant, υ is light frequency, and A is a constant. n is an index which depends on the electronic transition of the semiconductor. As for $BiVO_4$, AgBr and Co_3O_4, n is 1/2 [16]. Based on Kubelka–Munk transformed reflectance spectra (Fig. 4b), the band gap energy of pure $BiVO_4$, $Co_3O_4/BiVO_4$, $Ag@AgBr/BiVO_4$ and $Ag@AgBr/BiVO_4/Co_3O_4$ can be estimated from the intercept of the tangent to the plot of $(\alpha h\upsilon)^2$ vs. radiation energy $(h\upsilon)$. As expected, E_g of different photocatalysts followed the order of pure $BiVO_4$ (2.41 eV) > $Co_3O_4/BiVO_4$ (2.38 eV)

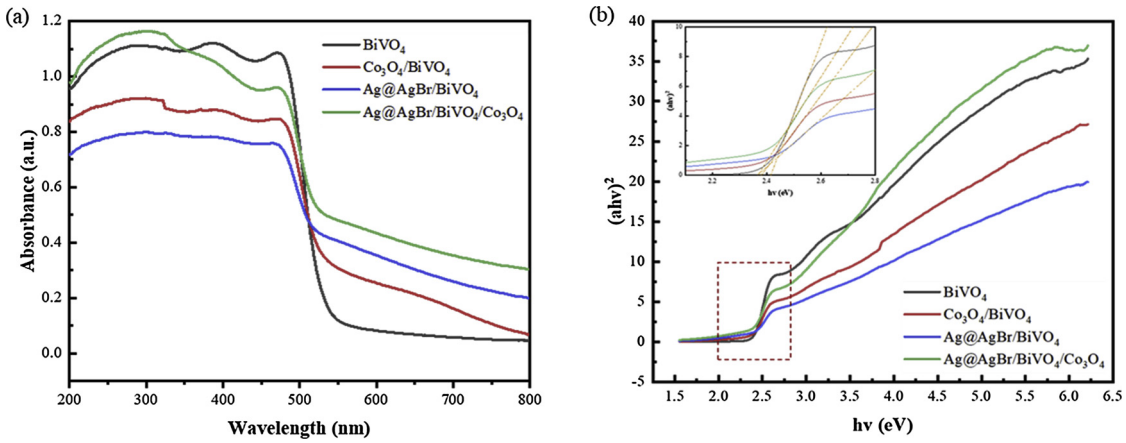

Fig. 4. (a) UV–vis DRS of $BiVO_4$, $Co_3O_4/BiVO_4$, $Ag@AgBr/BiVO_4$ and $Ag@AgBr/BiVO_4/Co_3O_4$(0.15 wt%); (b) The bandgap values of photocatalysts are determined by the corresponding Kubelka-Munk transformed reflectance spectra.

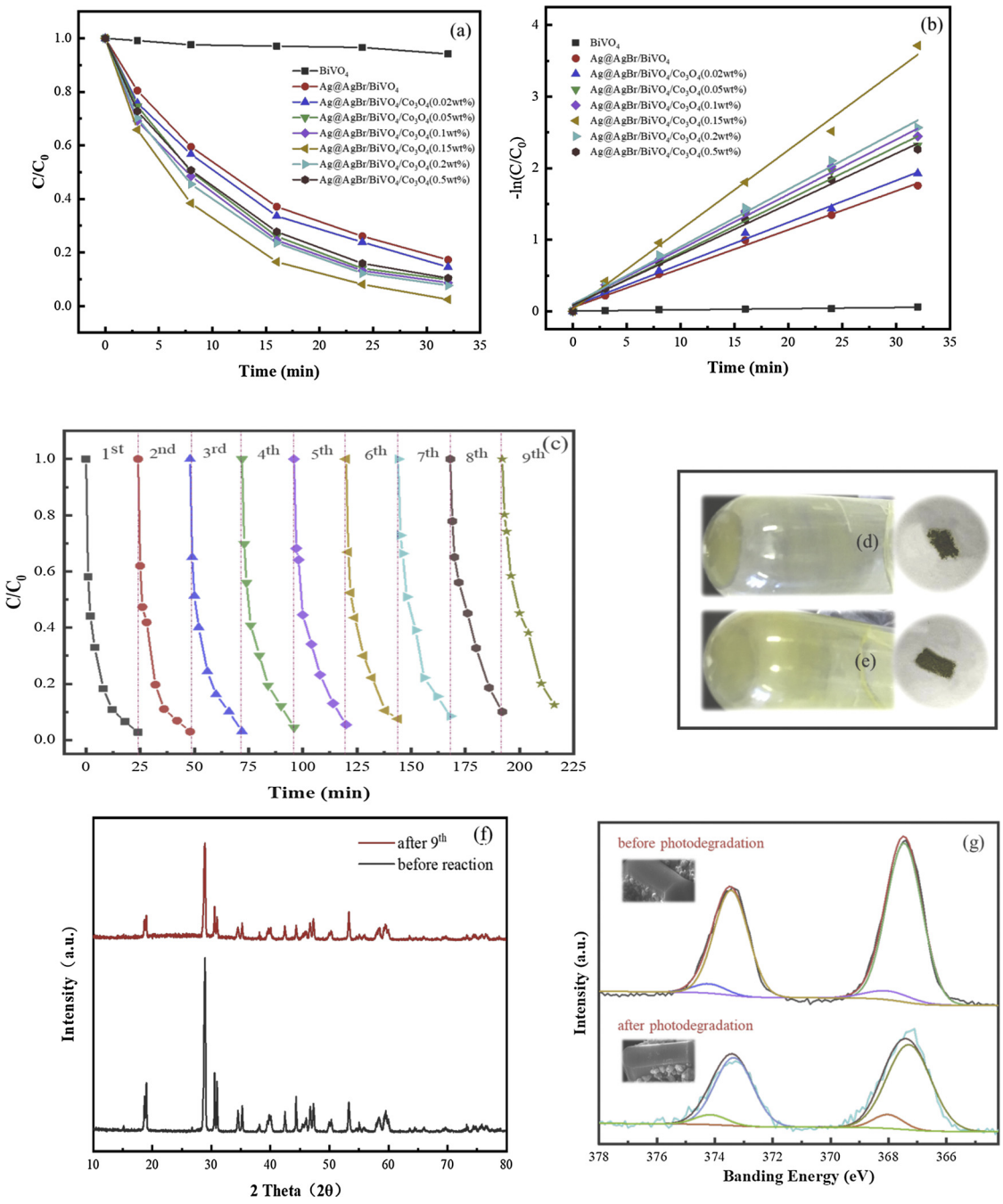

Fig. 5. (a) Photo-degradation of RhB over different synthesized samples; (b) Pseudo-first-order kinetic model fit the degradation kinetic curves of RhB; (c) Successive cycles photo-degradation of OTC over Ag@AgBr/$BiVO_4$/Co_3O_4(0.15 wt%); (d) and (e) are the color of Ag@AgBr/$BiVO_4$/Co_3O_4(0.15 wt%) before and after 9th recycling photodegradation of OTC; (f) XRD patterns of Ag@AgBr/$BiVO_4$/Co_3O_4(0.15 wt%) before and after 9th recycling photodegradation of OTC; (g) Ag 3d XPS spectra of Ag@AgBr/$BiVO_4$/Co_3O_4(0.15 wt%) before and after 9th recycling photodegradation of OTC.

> Ag@AgBr/$BiVO_4$ (2.36 eV) and Ag@AgBr/$BiVO_4$/Co_3O_4 (2.36 eV). Thus, Ag@AgBr/$BiVO_4$/Co_3O_4 could generate more electron-hole pairs under visible-light excitation. In addition, EPR and free radicals trapping experiments will be conducted to further confirm the Z-scheme structure of Ag@AgBr/$BiVO_4$/Co_3O_4, which will be discussed in details (Section (3.6).

3.3. Evaluation of photocatalytic activity

To evaluate the photocatalyst activity, photo-degradation of RhB (a typical organic dye) under visible-light irradiation is performed (Fig. 5a). The photo-degradation rates of RhB over different photocatalysts followed the order of Ag@AgBr/$BiVO_4$/Co_3O_4(0.15 wt %) > Ag@AgBr/$BiVO_4$/Co_3O_4(0.2 wt%) > Ag@AgBr/$BiVO_4$/Co_3O_4(0.1 wt%) > Ag@AgBr/$BiVO_4$/Co_3O_4(0.05 wt%) > Ag@AgBr/$BiVO_4$/Co_3O_4(0.5 wt%) > Ag@AgBr/$BiVO_4$/Co_3O_4(0.02 wt %) > Ag@AgBr/$BiVO_4$ > $BiVO_4$. Among them, Ag@AgBr/$BiVO_4$/Co_3O_4(0.15 wt%) possessed the highest visible-light photo-degradation rate of RhB. In addition, 65% of the total organic carbon (TOC) of RhB could be removed over Ag@AgBr/$BiVO_4$/Co_3O_4(0.15 wt%) within the 32 min (Fig. S4). Such enhancement of photocatalytic activity might be explained as follows: (1) introduction of Ag@AgBr could extend visible-light-responsive range of photocatalyst so as to generation of more electron-hole pairs under visible-light excitation; (2) construction of Z-

Table 1
The pseudo-first-order kinetic equations, rate constants (k) and regression coefficients (R^2) of photocatalytic degradation of RhB over as-synthesized samples.

Series	Photocatalyst	The first order kinetic equation	k(min^{-1})	R^2
1	$BiVO_4$	$-\ln(C/C_0) = 0.0016\,t$	0.0016	0.9104
2	Ag@AgBr/ $BiVO_4$	$-\ln(C/C_0) = 0.0549\,t$	0.0549	0.9946
3	Ag@AgBr/$BiVO_4$/Co_3O_4(0.02 wt%)	$-\ln(C/C_0) = 0.0584\,t$	0.0584	0.9927
4	Ag@AgBr/$BiVO_4$/Co_3O_4(0.05 wt%)	$-\ln(C/C_0) = 0.0741\,t$	0.0741	0.9879
5	Ag@AgBr/$BiVO_4$/Co_3O_4(0.1 wt%)	$-\ln(C/C_0) = 0.1012\,t$	0.1012	0.9901
6	Ag@AgBr/$BiVO_4$/Co_3O_4(0.15 wt%)	$-\ln(C/C_0) = 0.1112\,t$	0.1112	0.9931
7	Ag@AgBr/$BiVO_4$/Co_3O_4(0.2 wt%)	$-\ln(C/C_0) = 0.0804\,t$	0.0804	0.9921
8	Ag@AgBr/$BiVO_4$/Co_3O_4(0.5 wt%)	$-\ln(C/C_0) = 0.0706\,t$	0.0706	0.9925

scheme not only promoted the photo-carriers separation but also achieved higher photocatalytic oxidation and reduction ability; (3) loading of co-catalyst (Co_3O_4) could both accelerate the degradation kinetics and improve the charge separation of photocatalyst. In addition, the photo-degradation kinetic curves are fit by the pseudo-first-order kinetics equation (Fig. 5b), and the rate constants are listed in Table 1. Among them, Ag@AgBr/$BiVO_4$/Co_3O_4(0.15 wt%) showed the highest rate constant which was about 68 and 2.1 times as high as that of pure $BiVO_4$ and Ag@AgBr/$BiVO_4$, respectively. To objectively evaluate the photocatalytic activity, Table S2 lists the various photocatalysts with similar systems reported in previous literatures, which also demonstrate the superiority of Ag@AgBr/$BiVO_4$/Co_3O_4.

From the view of the practical application, the photocatalytic stability of Ag@AgBr/$BiVO_4$/Co_3O_4(0.15 wt%) was evaluated by 9 successive cycles degradation of OTC (10 $mg{\cdot}L^{-1}$) solutions. As expected, Ag@AgBr/$BiVO_4$/Co_3O_4(0.15 wt%) exhibits excellent photocatalytic stability (Fig. 5c). Even after the 9th cycle use, it could still remove more than 90% of OTC within 24 min. Furthermore, no obvious changes of the characteristic peaks of Ag@AgBr/$BiVO_4$/Co_3O_4(0.15 wt %) are observed in XRD pattern after photocatalytic reaction (Fig. 5f), which also show a stable crystal structure. In addition, the relative area ratio of Ag 3d peaks (Ag°/Ag^{+} = 18.5) is not changed after photocatalytic reaction (Fig. 5g), which further confirms that Ag^{+} is not reduced to Ag°. Thus, Ag@AgBr/$BiVO_4$/Co_3O_4(0.15 wt%) achieved excellent visible-light photocatalytic activity and anti-photocorrison ability.

3.4. Co-catalytic effect of Co_3O_4

The photo-degradation rate of RhB increased with the Co_3O_4 content of Ag@AgBr/$BiVO_4$/Co_3O_4 (Fig. 5a), and achieve the highest degradation rate of RhB as the Co_3O_4 content is 0.15 wt% (Table 1). The formation of built-in electric fields between the interface of Co_3O_4 and $BiVO_4$ could provide a strong driving force, which facilitated the separation of photo-electrons to {010} facets and holes to {110} facets. In addition, due to strong hole-sink effect, Co_3O_4 could promote the migration of holes from VB of $BiVO_4$ to Co_3O_4. Thus, selective deposition of Co_3O_4 on $BiVO_4${110} facets efficiently improved the photo-carriers separation.

Such co-catalytic effect of Co_3O_4 could be well proved by the photoluminescence (PL) spectra, photocurrent versus the irradiation time (I–t) curves and electrochemical impedance spectroscopy (EIS). Since PL emission arisen from the recombination of photo-generated carriers, the PL spectra could be used to evaluate the separation efficiency of electron-hole pairs in a photocatalyst [13]. Pure $BiVO_4$ exhibited strong emissions from 450 to 570 nm as it was excited at 278 nm. After introduction of Co_3O_4 and Ag@AgBr into $BiVO_4$, the PL peak was obviously weakened. The PL intensities of the photocatalysts followed the order of $BiVO_4$ > Ag@AgBr/$BiVO_4$ > Ag@AgBr/$BiVO_4$/Co_3O_4(0.15 wt %) (Fig. 6a), which is in accordance with the photocatalytic performances. In general, the weaker PL signal means the higher separation efficiency of photo-generated carriers. The lowest peak intensity of Z-scheme structured Ag@AgBr/$BiVO_4$/Co_3O_4(0.15 wt%) suggested that photo-generated electrons and holes could be efficiently transferred from $BiVO_4$ to Ag nanoparticles and Co_3O_4, respectively. On the other hand, due to successful construction of Z-scheme structure, photo-electrons of $BiVO_4$ can be efficiently transferred to Ag° and subsequently recombined with photo-generated holes of AgBr. Such recombination of photo-carriers in Ag° still generated the fluorescence of Ag@AgBr/$BiVO_4$/Co_3O_4 to a certain extent. The similar phenomenon was also found in g-C_3N_4@Ag/$BiVO_4$(040) [46]. Besides, the photo current transient response measurement is also used to evaluate the separation efficiency of photo-generated carriers of photocatalysts (Fig. 6b). As expected, Ag@AgBr/$BiVO_4$/Co_3O_4(0.15 wt%) displayed the highest photocurrent intensity (2.16 μA cm^{-2}) which is about 21, 6 and 2 times higher than that of pure $BiVO_4$ (0.1 μA cm^{-2}), Co_3O_4/$BiVO_4$ (0.35 μA cm^{-2}) and Ag@AgBr/BiVO4 (0.93 μA cm^{-2}), respectively. This result is consistent with the PL experiments. In addition, electrochemical impedance spectrum (EIS) measurements showed the lowest charge transfer resistance of Ag@AgBr/$BiVO_4$/Co_3O_4(0.15 wt%) (Fig. 6c), also suggesting a higher electron-hole pairs separation efficiency than $BiVO_4$, Co_3O_4/$BiVO_4$ and Ag@AgBr/BiVO4.

Thus, the strong hole-sink effect of Co_3O_4 and built-in electric fields between Co_3O_4 and $BiVO_4$ strengthened the 'pre-separation channel effect' of $BiVO_4$, resulting in the significant improvement of the photo-carriers separation of Z-scheme structured Ag@AgBr/$BiVO_4$/Co_3O_4.

3.5. Possible degradation pathway of OTC

To identify the photo-degradation intermediates of OTC, iron spectra at different retention time (RT) of OTC under visible-light irradiation (0, 2, 3, 4 and 8 min) are recorded in ESI Scan (Fig. S2). Before visible-light irradiation, typical ions spectra {m/z = 461 ($[M+H]^{+}$)} of OTC at RT = 8.5 min was detected in solution. After visible-light irradiation, eight ions spectra appeared at RT = 4.518–9.806 min. These main product ions at m/z = 449 ($[M+H]^{+}$), m/z = 443 ($[M+H]^{+}$), m/z = 433 ($[M+H]^{+}$), m/z = 415 ($[M+H]^{+}$), m/z = 370.7 ($[M+H]^{+}$), m/z = 304.2 ($[M+H]^{+}$), m/z = 203 ($[M+H]^{+}$) and m/z = 119.3 ($[M+H]^{+}$) might be identified as $C_{21}H_{22}N_2O_9$, $C_{20}H_{20}N_2O_9$, $C_{22}H_{22}N_2O_8$, $C_{20}H_{18}N_2O_8$, $C_{19}H_{19}NO_7$, $C_{17}H_{20}O_5$, $C_{12}H_{10}O_3$ and $C_{11}H_{12}O_3$, respectively. Based on the LC–MS/TOF results and previous literatures [47–55], the possible photo-degradation pathways of OTC are proposed (Scheme 1).

3.6. Photocatalytic mechanism

The free radicals trapping experiments of Ag@AgBr/$BiVO_4$/Co_3O_4 composite were conducted to determine the main reactive species, which could further illustrate the photocatalytic degradation mechanism. In the photodegradation process of RhB, the hole (h^{+}) scavenger (EDTA-2Na), hydroxyl radical (·OH) scavenger (BuOH) and superoxide radical ($\cdot O_2^{-}$) scavenger (BQ) were respectively added in the reaction system. It is found that BuOH has little impact on photo-degradation of RhB while EDTA-2Na and BQ obviously inhibit the RhB degradation (Fig. 7a). Therefore, it can be concluded that both h^{+} and $\cdot O_2^{-}$ are the main active species in the suspension of Ag@AgBr/$BiVO_4$/

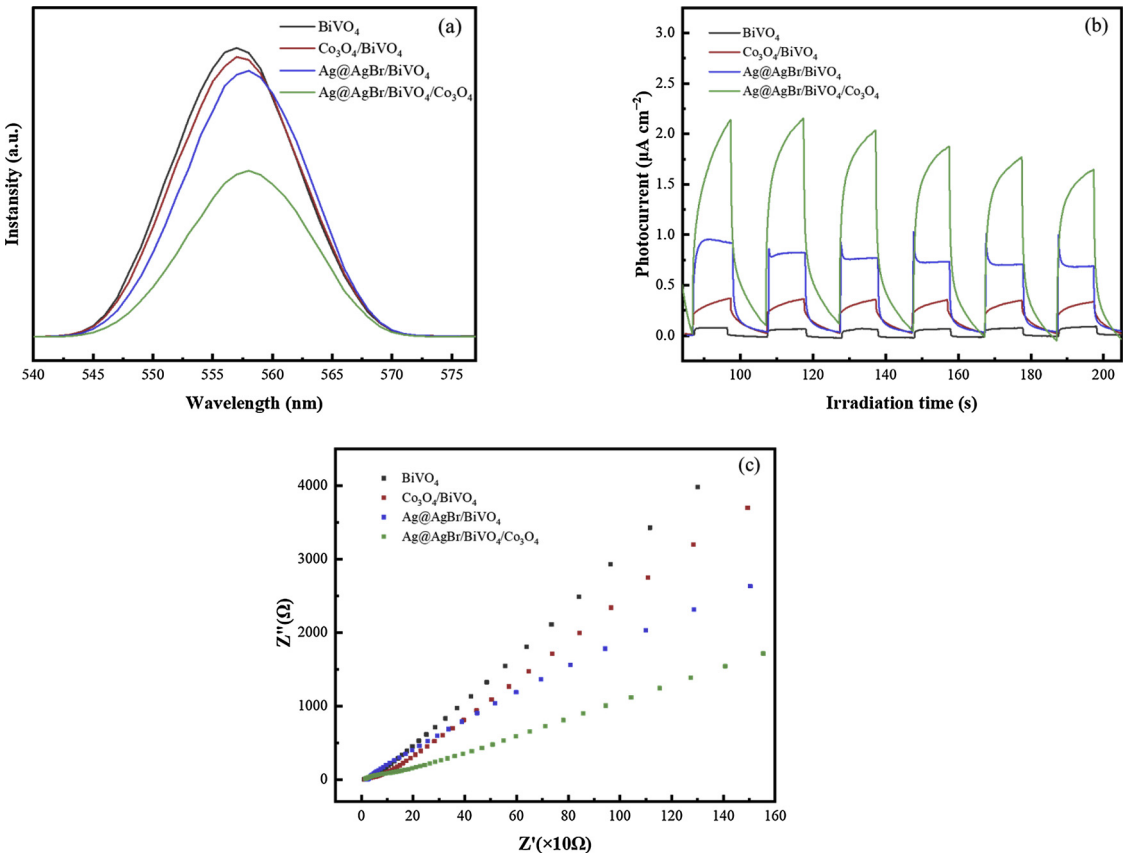

Fig. 6. (a) Photoluminescence spectra of pure $BiVO_4$, $Co_3O_4/BiVO_4$, Ag@AgBr/$BiVO_4$ and Ag@AgBr/$BiVO_4/Co_3O_4$(0.15 wt%) composites; (b)Photocurrent response for the pure $BiVO_4$, $Co_3O_4/BiVO_4$, Ag@AgBr/$BiVO_4$ and Ag@AgBr/$BiVO_4/Co_3O_4$(0.15 wt%) composites; (c) Electrochemical impedance spectroscopy (EIS) Nyquist plots of the sample electrodes of the pure $BiVO_4$, $Co_3O_4/BiVO_4$, Ag@AgBr/$BiVO_4$ and Ag@AgBr/$BiVO_4/Co_3O_4$(0.15 wt%) composites.

Co_3O_4 under visible-light irradiation. Notably, the generation of $^{\cdot}O_2^-$ further confirmed the successful construction of Z-scheme structured Ag@AgBr/$BiVO_4/Co_3O_4$. This is because if AgBr and $BiVO_4$ constructed the heterojunction (Scheme 2a), the electrons photoinduced from the CB of AgBr would transfer to the CB of $BiVO_4$, and the holes photogenerated from the VB of $BiVO_4$ would transfer to the VB of AgBr. However, the electrons on the CB of $BiVO_4$ cannot reduce O_2 to $^{\cdot}O_2^-$ because of more positive CB potential of $BiVO_4$ (+0.11 eV vs NHE) than $E^{\circ}(O_2/^{\cdot}O_2^-)$ (−0.046 eV vs NHE). Thus, deposition of Ag@AgBr on $BiVO_4${010} did not construct the heterojunction but construct the Z-scheme structure.

As for Z-scheme structured Ag@AgBr/$BiVO_4/Co_3O_4$, the electrons photoinduced from the CB of $BiVO_4$ would be transferred to Ag° and subsequently recombined with holes photogenerated from the VB of AgBr. Since the energy level of electrons on the CB of AgBr (−0.30 eV vs NHE) is sufficient negative to reduce O_2 to $^{\cdot}O_2^-$, the transfer route of photoinduced electrons and holes in the Ag@AgBr/$BiVO_4/Co_3O_4$ composites follow the Z-scheme with Ag° served as electron mediator (Scheme 2b). To confirm the Z-scheme structure of Ag@AgBr/$BiVO_4$/Co_3O_4 and Ag@AgBr/$BiVO_4$, EPR (detection of DMPO-$^{\cdot}O_2^-$) are conducted over different catalysts ($BiVO_4$, $Co_3O_4/BiVO_4$, Ag@AgBr/$BiVO_4$ and Ag@AgBr/$BiVO_4/Co_3O_4$) in methanol solution under visible-light (Fig. 7b). As a result, DMPO-$^{\cdot}O_2^-$ signals are detected only over Ag@AgBr/$BiVO_4$ and Ag@AgBr/$BiVO_4/Co_3O_4$, while there are no DMPO-$^{\cdot}O_2^-$ signals detected over $BiVO_4$ and $Co_3O_4/BiVO_4$. Thus, deposition of Ag@AgBr on $BiVO_4${010} can construct the Z-scheme structure.

Based on the above research, the possible photocatalytic mechanism of Z-scheme structured Ag@AgBr/$BiVO_4/Co_3O_4$ is proposed (Scheme 2b). Ag@AgBr doped onto $BiVO_4$ {010} facets could construct the Z-scheme structure for promotion of photocarriers separation via more optimum transfer channels. Under visible-light irradiation, the VB electrons of $BiVO_4$ and AgBr are excited to their CB. Due to the different energy levels of the CB and VB between {010} and {110} facets, $BiVO_4$ could act as the 'pre-separation channel' to achieve spatial charge separation, which facilitated the accumulation of electrons on {010} facets and holes on {110} facets. Here Ag° could not only improve the utilization of visible-light due to SPR-effect, but also serve as the recombination center of charge carriers in Z-scheme structured Ag@AgBr/$BiVO_4/Co_3O_4$. The photo-electron on the CB of $BiVO_4$ {010} facets and holes on the VB of AgBr are recombined at Ag°, resulting in the accumulation of photo-electron on the CB of AgBr and holes on the VB of $BiVO_4$. As deriving-hole-type co-catalyst, Co_3O_4 could capture the photo-generated holes on $BiVO_4${110} facet for subsequent oxidation of organics. Thus, the synergistic effect of Z-scheme structure, pre-separation channel and deriving-hole-type co-catalyst significantly improved the photogenerated charge separation. On the other hand, the photo-electrons on the CB of AgBr could reduce the O_2 to $^{\cdot}O_2^-$ which also played important role in organics degradation. The deriving-hole-type co-catalyst Co_3O_4 could also catalyze the oxidation reaction by lowering the activation energy. Thus, Ag@AgBr/$BiVO_4/Co_3O_4$(0.15 wt %) exhibited excellent photocatalytic activity and stability.

4. Conclusions

Highly efficient Z-scheme structured visible-light photocatalyst was constructed by selective deposition of Ag@AgBr and Co_3O_4 separately on {010} and {110} facet of $BiVO_4$. In Ag@AgBr/$BiVO_4/Co_3O_4$ composite, $BiVO_4$ can act as a 'pre-separation channel' to achieve spatial charge separation because of the different energy levels of CB and VB between {010} and {110} facets. Ag@AgBr doped onto $BiVO_4$ {010} facets could construct the Z-scheme structure for promotion of

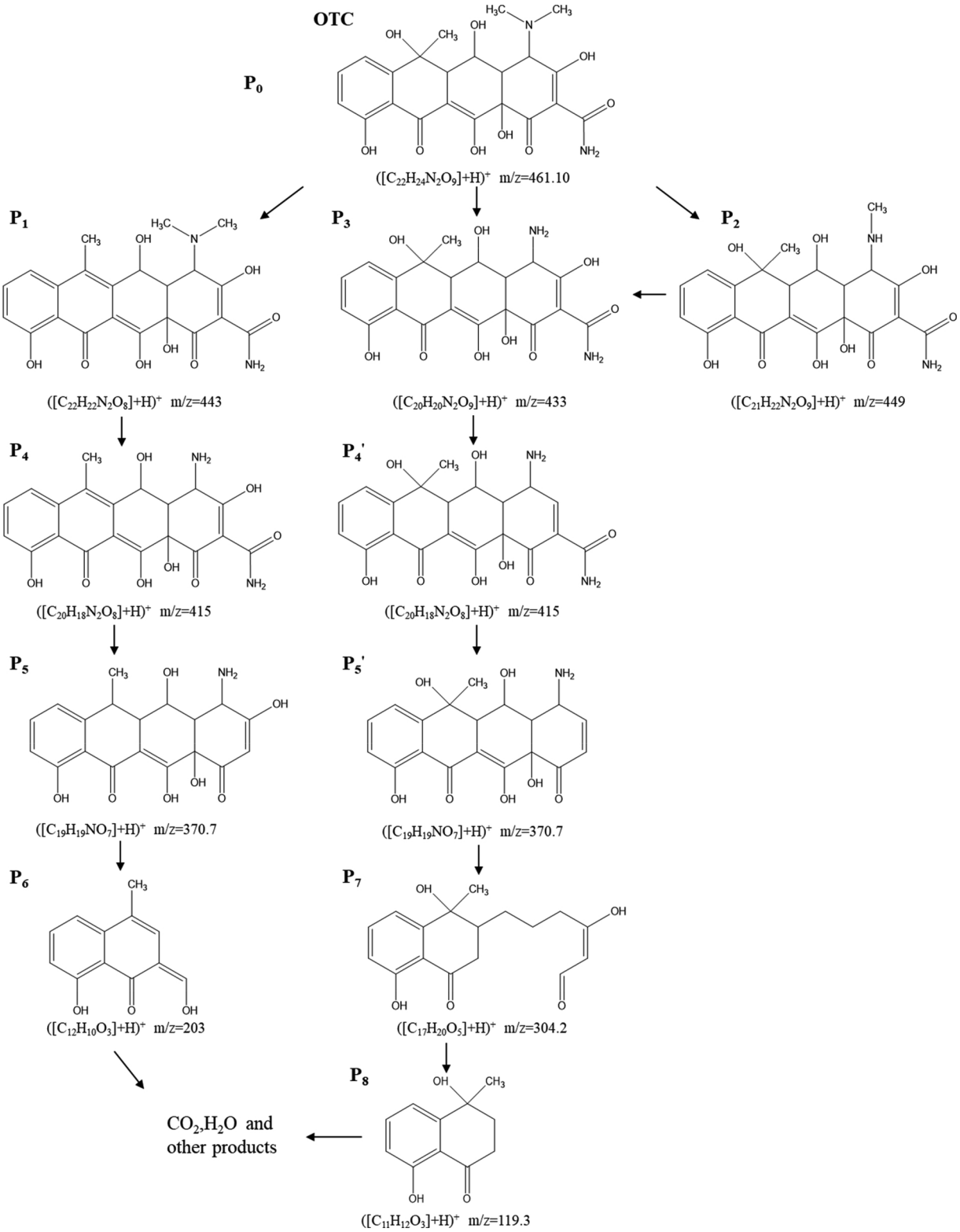

Scheme 1. Proposed photodegradation pathways of OTC over Ag@AgBr/$BiVO_4$/Co_3O_4(0.15 wt%).

photocarriers separation via more optimum transfer channels. Meanwhile, as the electron mediator of Z-scheme, Ag° could also enhance the visible-light utilization due to SPR-effect. On the other hand, as deriving-hole-type co-catalysts, Co_3O_4 could capture the photo-generated holes of $BiVO_4${110} facet for organics oxidation. Thus, the Z-scheme structured Ag@AgBr/$BiVO_4$/Co_3O_4(0.15 wt%) achieved high visible-light photocatalytic activity and stability. Both h^+ and $\cdot O_2^-$ are the main active species for organics oxidation under visible-light irradiation. In addition, the possible photo-degradation pathway and intermediate of OTC were proposed. In summary, this work not only prepared a highly efficient visible-light photocatalyst for organics degradation, but also provided a new method to construct Z-scheme structured photocatalysts with pre-separation channel and hole-sink effects.

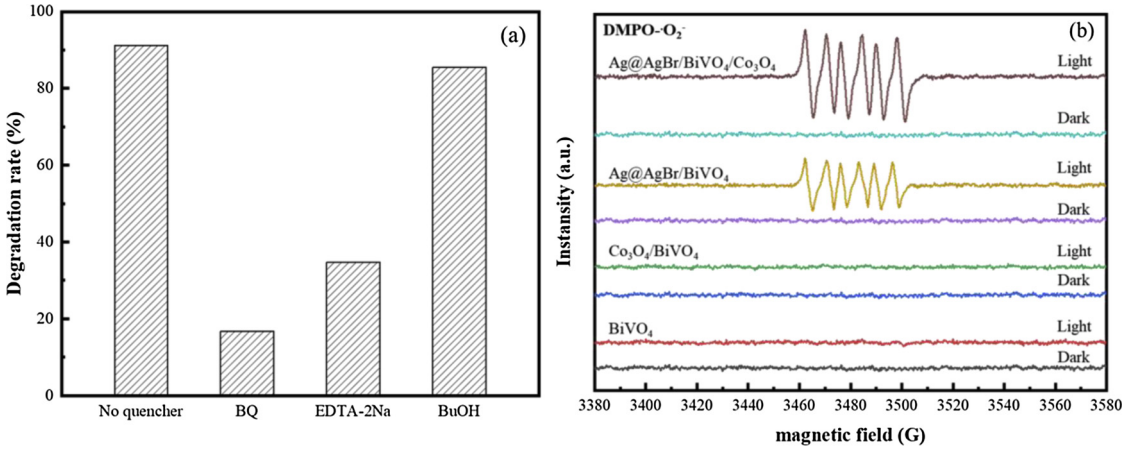

Fig. 7. (a) Trapping experiment of active species during the photo-degradation of RhB over Ag@AgBr/$BiVO_4$ /Co_3O_4 under visible light irradiation; (b) EPR signals over $BiVO_4$, Co_3O_4/$BiVO_4$, Ag@AgBr/$BiVO_4$ and Ag@AgBr/$BiVO_4$/Co_3O_4.

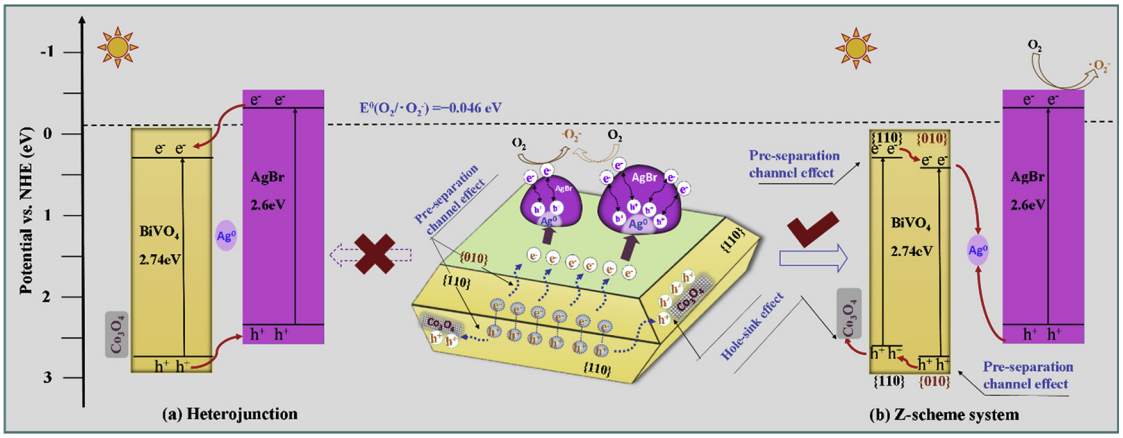

Scheme 2. Photocatalytic mechanism of Ag@AgBr/$BiVO_4$/Co_3O_4.

Acknowledgements

This research was supported by Natural Science Foundation of China (No. 51878335) and the Fundamental Research Funds for the Central Universities (0211-14380085). We also acknowledge the support provided by the Key Program of Natural Science Foundation of China (No. 51438008).

Appendix A. Supplementary data

Supplementary material related to this article can be found, in the online version, at doi:https://doi.org/10.1016/j.apcatb.2019.03.023.

References

[1] C. Liang, C.G. Niu, L. Zhang, X.J. Wen, S.F. Yang, H. Guo, G.M. Zeng, J. Hazard. Mater. 361 (2019) 245–258.
[2] X. Meng, Z. Zhang, J. Mol. Catal. A: Chem. 423 (2016) 533–549.
[3] M. Pálmai, E.M. Zahran, S. Angaramo, S. Bálint, Z. Pászti, M.R. Knecht, L.G. Bachas, J. Mater. Chem. A 5 (2017) 529–534.
[4] H.L. Tan, R. Amal, Y.H. Ng, J. Mater. Chem. A 5 (2017) 16498–16521.
[5] L. Ye, Y. Su, X. Jin, H. Xie, C. Zhang, Environ. Sci. Nano 1 (2014) 90.
[6] T. Cai, Y. Liu, L. Wang, S. Zhang, Y. Zeng, J. Yuan, J. Ma, W. Dong, C. Liu, S. Luo, Appl. Catal. B-Environ. 208 (2017) 1–13.
[7] H. Guo, C.-G. Niu, D.-W. Huang, N. Tang, C. Liang, L. Zhang, X.-J. Wen, Y. Yang, W.-J. Wang, G.-M. Zeng, Chem. Eng. J. 360 (2019) 349–363.
[8] H. Guo, H.-Y. Niu, C. Liang, C.-G. Niu, D.-W. Huang, L. Zhang, N. Tang, Y. Yang, C.-Y. Feng, G.-M. Zeng, J. Catal. 370 (2019) 289–303.
[9] M. Li, Y. Dai, X. Ma, T. Jing, B. Huang, Appl. Catal. B-Environ. 205 (2017) 211–218.
[10] N. Shao, Z. Hou, H. Zhu, J. Wang, C.P. François-Xavier, Appl. Catal. B-Environ. 232 (2018) 574–586.
[11] H. Yu, W. Chen, X. Wang, Y. Xu, J. Yu, Appl. Catal. B-Environ. 187 (2016) 163–170.
[12] F.F. Abdi, N. Firet, R. van de Krol, ChemCatChem 5 (2013) 490–496.
[13] F. Chen, Q. Yang, X. Li, G. Zeng, D. Wang, C. Niu, J. Zhao, H. An, T. Xie, Y. Deng, Appl. Catal. B-Environ. 200 (2017) 330–342.
[14] W. Zhao, Y. Liu, Z. Wei, S. Yang, H. He, C. Sun, Appl. Catal. B-Environ. 185 (2016) 242–252.
[15] Z. Wei, D. Benlin, Z. Fengxia, T. Xinyue, X. Jiming, Z. Lili, L. Shiyin, D.Y.C. Leung, C. Sun, Appl. Catal. B-Environ. 229 (2018) 171–180.
[16] Y. Liu, J. Kong, J. Yuan, W. Zhao, X. Zhu, C. Sun, J. Xie, Chem. Eng. J. 331 (2018) 242–254.
[17] T.S. Natarajan, K.R. Thampi, R.J. Tayade, Appl. Catal. B-Environ. 227 (2018) 296–311.
[18] P. Zhou, J. Yu, M. Jaroniec, Adv. Mater. 26 (2014) 4920–4935.
[19] H. Li, W. Tu, Y. Zhou, Z. Zou, Adv. Sci. (Weinh.) 3 (2016) 1500389.
[20] P. Wang, B. Huang, X. Qin, X. Zhang, Y. Dai, J. Wei, M.-H. Whangbo, Angew. Chem. 120 (2008) 8049–8051.
[21] Y. Bi, J. Ye, Chem. Eur. J. 16 (2010) 10327–10331.
[22] H. Li, S. Gan, H. Wang, D. Han, L. Niu, Adv. Mater. 27 (2015) 6906–6913.
[23] X. Li, S. Fang, L. Ge, C. Han, P. Qiu, W. Liu, Appl. Catal. B-Environ. 176–177 (2015) 62–69.
[24] F. Chen, Q. Yang, Y. Wang, F. Yao, Y. Ma, X. Huang, X. Li, D. Wang, G. Zeng, H. Yu, Chem. Eng. J. 348 (2018) 157–170.
[25] L. Zhang, Y. Shi, L. Wang, C. Hu, Appl. Catal. B-Environ. 220 (2018) 118–125.
[26] F. Chen, Q. Yang, Y. Wang, J. Zhao, D. Wang, X. Li, Z. Guo, H. Wang, Y. Deng, C. Niu, G. Zeng, Appl. Catal. B-Environ. 205 (2017) 133–147.
[27] H. Guo, C.G. Niu, X.J. Wen, L. Zhang, C. Liang, X.G. Zhang, D.L. Guan, N. Tang, G.M. Zeng, J. Colloid Interface Sci. 513 (2018) 852–865.
[28] H. Li, Y. Sun, B. Cai, S. Gan, D. Han, L. Niu, T. Wu, Appl. Catal. B-Environ. 170–171 (2015) 206–214.
[29] Q. Liu, C. Zeng, L. Ai, Z. Hao, J. Jiang, Appl. Catal. B-Environ. 224 (2018) 38–45.
[30] P. Wang, B. Huang, X. Zhang, X. Qin, H. Jin, Y. Dai, Z. Wang, J. Wei, J. Zhan, S. Wang, J. Wang, M.-H. Whangbo, Chem. Eur. J. 15 (2009) 1821–1824.
[31] X.-J. Wen, C.-G. Niu, L. Zhang, C. Liang, H. Guo, G.-M. Zeng, J. Catal. 358 (2018) 141–154.
[32] J. He, Y. Cheng, T. Wang, D. Feng, L. Zheng, D. Shao, W. Wang, W. Wang, F. Lu, H. Dong, R. Zheng, H. Liu, Appl. Surf. Sci. 440 (2018) 99–106.
[33] L. Zhang, W. Feng, B. Wang, K. Wang, F. Gao, Y. Zhao, P. Liu, Appl. Catal. B-

Environ. 212 (2017) 80–88.
[34] R. Li, F. Zhang, D. Wang, J. Yang, M. Li, J. Zhu, X. Zhou, H. Han, C. Li, Nat. Commun. 4 (2013) 1432.
[35] J. Yang, D. Wang, H. Han, C. Li, Acc. Chem. Res. 46 (2013) 1900–1909.
[36] L. Ye, X. Liu, Q. Zhao, H. Xie, L. Zan, J. Mater. Chem. A 1 (2013) 8978.
[37] F. Lin, Y. Zhang, L. Wang, Y. Zhang, D. Wang, M. Yang, J. Yang, B. Zhang, Z. Jiang, C. Li, Appl. Catal. B-Environ. 127 (2012) 363–370.
[38] C. Tang, E. Liu, J. Wan, X. Hu, J. Fan, Appl. Catal. B-Environ. 181 (2016) 707–715.
[39] R. Li, H. Han, F. Zhang, D. Wang, C. Li, Energy Environ. Sci. 7 (2014) 1369–1376.
[40] B. Ma, J. Guo, W.-L. Dai, K. Fan, Appl. Catal. B-Environ. 130–131 (2013) 257–263.
[41] Y. Zhang, Z.-R. Tang, X. Fu, Y.-J. Xu, Appl. Catal. B-Environ. 106 (2011) 445–452.
[42] Y. Wang, G. Tan, T. Liu, Y. Su, H. Ren, X. Zhang, A. Xia, L. Lv, Y. Liu, Appl. Catal. B-Environ. 234 (2018) 37–49.
[43] S. Xiong, J.S. Chen, X.W. Lou, H.C. Zeng, Adv. Funct. Mater. 22 (2012) 861–871.
[44] C. Han, L. Ge, C. Chen, Y. Li, X. Xiao, Y. Zhang, L. Guo, Appl. Catal. B-Environ. 147 (2014) 546–553.
[45] J. He, D.W. Shao, L.C. Zheng, L.J. Zheng, D.Q. Feng, J.P. Xu, X.H. Zhang, W.C. Wang, W.H. Wang, F. Lu, H. Dong, Y.H. Cheng, H. Liu, R.K. Zheng, Appl. Catal. B-Environ. 203 (2017) 917–926.
[46] M. Ou, S. Wan, Q. Zhong, S. Zhang, Y. Song, L. Guo, W. Cai, Y. Xu, Appl. Catal. B-Environ. 221 (2018) 97–107.
[47] S. Jiao, S. Zheng, D. Yin, L. Wang, L. Chen, J. Environ. Sci. 20 (2008) 806–813.
[48] J.H.O.S. Pereira, V.J.P. Vilar, M.T. Borges, O. González, S. Esplugas, R.A.R. Boaventura, Sol. Energy 85 (2011) 2732–2740.
[49] F. Yuan, C. Hu, X. Hu, D. Wei, Y. Chen, J. Qu, J. Hazard. Mater. 185 (2011) 1256–1263.
[50] R. Li, Y. Jia, J. Wu, Q. Zhen, RSC Adv. 5 (2015) 40764–40771.
[51] Q. Chen, S. Wu, Y. Xin, Chem. Eng. J. 302 (2016) 377–387.
[52] W.-K. Jo, S. Kumar, M.A. Isaacs, A.F. Lee, S. Karthikeyan, Appl. Catal. B-Environ. 201 (2017) 159–168.
[53] N. Shao, J. Wang, D. Wang, P. Corvini, Appl. Catal. B-Environ. 203 (2017) 964–978.
[54] J. Xu, Z. Bian, X. Xin, A. Chen, H. Wang, Chem. Eng. J. 337 (2018) 684–696.
[55] B. Zhou, Y. Li, J. Bai, X. Li, F. Li, L. Liu, Appl. Surf. Sci. 464 (2019) 115–124.